Minimum inverter capacity design for LC-hybrid active power filters in three-phase four-wire distribution systems

C.-S. Lam[1]   X.-X. Cui[1]   W.-H. Choi[1]   M.-C. Wong[1]   Y.-D. Han[1,2]

[1]Department of Electrical and Computer Engineering, University of Macau, Macao, People's Republic of China
[2]Department of Electrical Engineering, Tsinghua University, Beijing, People's Republic of China
E-mail: C.S.Lam@ieee.org

Abstract: This study presents a minimum inverter capacity design for three-phase four-wire centre-split inductor-capacitor (LC) coupling hybrid active power filters (LC-HAPFs). Based on its equivalent circuit models in $d-q-0$ coordinate, the coupling part filtering characteristics of the LC-HAPF without or with neutral inductor can be more clearly illustrated and easily understood, compared with the past analysis based on the generic filter structure. According to the current quality data, the minimum dc-link voltage expressions for the LC-HAPF without and with neutral inductor are deduced and compared. Conventionally, the coupling LC is usually tuned at a higher fifth- or seventh-order harmonic frequency to reduce its cost and size compared with third-order case. When triplen harmonic currents exist significantly, the LC-HAPF with a small tuned neutral inductor can further reduce its minimum dc-link voltage requirement. Thus, the initial cost, switching loss and switching noise of the LC-HAPF can be lowered. Representative simulation and experimental results of the three-phase four-wire LC-HAPF with neutral inductor are presented to verify the filtering characteristics analysis and minimum dc-link voltage expressions, to show the effectiveness of reducing its inverter capacity, switching loss and switching noise in current quality compensation compared with the conventional LC-HAPF.

1 Introduction

Nowadays, because of the rapid growth of advanced power conversion devices and power electronic equipments, their full wave rectifier front-ends make the power quality issues become more serious, especially in harmonic current (3rd, 5th, 7th, 9th etc.) and reactive power problems. High current harmonic distortion causes various problems in both distribution systems and consumer products, such as equipment overheating, blown capacitor fuses, mal-operation of the protection devices, transformer overheating and so on [1, 2]. The triplen harmonic currents (especially third order) drawn by these rectifier front ends will accumulate in the neutral conductor, which results in increasing the risk for stray voltage complaints especially near substations and the electromagnetic field (EMF) levels near three-phase distribution feeders [3]. Excess neutral current will also overheat and even burn the neutral conductor. In addition, the rectifier front-ends usually accompany with low-power factor problem as well. The larger the reactive current/power, the larger the system losses and the lower the network stability. Owing to these reasons, electrical utilities usually charge the industrial and commercial customers a higher electricity cost with low-power factor situation.

To eliminate those harmonic current and reactive power problems, power filters can be implemented. Since the first installation of passive power filters (PPFs) in the mid-1940s,

PPFs have been widely used to suppress harmonic current and compensate reactive power in distribution power systems [4–7] because of their low cost, simplicity and high efficiency characteristics. Unfortunately, they have many disadvantages such as low dynamic performance, filtering characteristics easily be affected by small variations of the system parameter values and resonance problems [4–6, 8–10]. Since the concept 'Active ac Power Filter' (APFs) was first developed by L. Gyugyi in 1976 [7, 11], the research studies of the APFs for current quality compensation are prospering since then. APFs can overcome the disadvantages inherent in PPFs, but the initial and operational costs are relatively high [4, 5, 8–16] because its dc-link operating voltage should be higher than the system voltage during inductive loading. This results in slowing down their large-scale application in distribution networks. Later on, different hybrid active power filter (HAPF) topologies composed of active and passive parts in series and/or parallel have been proposed, aiming to improve the compensation characteristics of PPFs and reduce the voltage and/or current ratings (costs) of the APFs, thus providing a cost-effective solution for compensating harmonic and reactive current problems [8–11, 14–24]. Among different HAPF topologies in [8–11, 14–19], a transformerless LC coupling HAPF (LC-HAPF) has been recently proposed, applied for current quality compensation and damping of harmonic propagation in distribution power systems [18, 20–23], in which it has less

passive components and lower dc-link operating voltage comparing with an APF [20]. In addition, the coupling LC is designed based on the fundamental reactive power consumption of the loading and tuned harmonic frequency. To reduce the cost and size compared with that tuned at the third-order case, they are conventionally tuned at the fifth- or seventh-order harmonic frequencies [17, 20–23]. In addition, the LC-HAPF should be switched off during no load or light load situations for preventing over-compensation.

To improve filtering performances for the coupling part of the three-phase four-wire LC-HAPF without adding any extra LC branches, the authors in [25] has presented an analysis for the LC-HAPF with a neutral inductor. Through the generic filter structure under positive, negative and zero-sequence analysis, instead of having only one filtering resonant frequency from the coupling LC, the LC-HAPF with a tuned neutral inductor can provide two different resonant frequencies simultaneously in order to predominantly drain harmonic current away at these two frequencies [25]. However, the coupling part filtering improvement analysis based on the generic filter structure is not as obvious and comprehensible as the deduced equivalent circuit models in $d-q-0$ coordinate in this paper. Moreover, because of the limitations among the existing literatures [21–25], there is still no mathematical deduction for the design of the LC-HAPF minimum dc-link voltage in current harmonics and reactive power compensation. Therefore the key contribution of this paper is to investigate and discuss the minimum dc-link voltage design for a three-phase four-wire LC-HAPF with and without neutral inductor. So that the inverter capacity reduction analysis by adding a neutral inductor can be mathematically found.

In the following, a transformerless two-level three-phase four-wire centre-split LC-HAPF and its corresponding equivalent circuit models in $d-q-0$ coordinate are initially introduced in Section 2. Based on these circuit models, its coupling part filtering characteristics without and with neutral inductor are analysed and discussed. According to the current quality of the loading and the LC-HAPF single-phase equivalent circuit models in $a-b-c$ coordinate, the minimum dc-link voltage expressions for the LC-HAPF without and with neutral inductor are proposed in Section 3. Finally, representative simulation and experimental results of the three-phase four-wire centre-split LC-HAPF with neutral inductor are given to verify its filtering characteristics and the minimum dc-link voltage design expressions, to show the effectiveness of reducing its dc-link voltage requirement, switching loss and switching noise in current quality compensation compared with the conventional LC-HAPF without neutral inductor. Given that most of the loadings in the distribution power systems are inductive, the following analysis and discussion only focus on inductive non-linear loads [26].

2 Mathematical modelling of a transformerless two-level three-phase four-wire centre-split LC-HAPF in $d-q-0$ coordinate

2.1 Equivalent circuit models of a three-phase four-wire LC-HAPF in $d-q-0$ coordinate

A transformerless two-level three-phase four-wire centre-split LC-HAPF with neutral inductor is shown in Fig. 1a, in which the non-linear loads can be modelled as three single-phase full bridge diode rectifiers. The corresponding equivalent circuit

model of LC-HAPF in $a-b-c$ coordinate is shown in Fig. 1b, where the subscript 'x' denotes phase a, b, c, n. v_x is the load voltage, i_{sx}, i_{Lx} and i_{cx} are the system, load and inverter current for each phase. C_c and L_c are the coupling part capacitor and inductor for each leg of the three-phase voltage source inverter (VSI). v_{Ccx} and v_{Lcx} are the coupling capacitor voltage and inductor voltage. L_n and v_{Ln} is the neutral inductor and neutral inductor voltage of the three-phase VSI. C_{dc} and V_{dc} are the dc capacitor, upper and lower dc capacitor voltages. The dc-link voltage is assumed as an ideal voltage source of $2V_{dc}$, and v_{invx} is the inverter output voltage.

From Fig. 1b, the differential equations of the coupling inductor L_c and capacitor C_c can be expressed as

$$L_c \frac{d}{dt} \begin{bmatrix} i_{ca} \\ i_{cb} \\ i_{cc} \end{bmatrix} = \begin{bmatrix} v_{inva} \\ v_{invb} \\ v_{invc} \end{bmatrix} + L_n \frac{d}{dt} \begin{bmatrix} i_{cn} \\ i_{cn} \\ i_{cn} \end{bmatrix} - \left(\begin{bmatrix} v_a \\ v_b \\ v_c \end{bmatrix} - \begin{bmatrix} v_{Cca} \\ v_{Ccb} \\ v_{Ccc} \end{bmatrix} \right) \tag{1}$$

$$C_c \frac{d}{dt} \begin{bmatrix} v_{Cca} \\ v_{Ccb} \\ v_{Ccc} \end{bmatrix} = - \begin{bmatrix} i_{ca} \\ i_{cb} \\ i_{cc} \end{bmatrix} \tag{2}$$

With the help of [27, 28], after applying Park transformation, (1) and (2) in the $d-q-0$ rotating coordinate can be expressed as

$$\omega L_c \begin{bmatrix} -i_{cq} \\ i_{cd} \\ 0 \end{bmatrix} + L_c \frac{d}{dt} \begin{bmatrix} i_{cd} \\ i_{cq} \\ i_{c0} \end{bmatrix} = \begin{bmatrix} v_{invd} \\ v_{invq} \\ v_{inv0} \end{bmatrix} - 3L_n \frac{d}{dt} \begin{bmatrix} 0 \\ 0 \\ i_{c0} \end{bmatrix}$$
$$- \left(\begin{bmatrix} v_d \\ v_q \\ v_0 \end{bmatrix} - \begin{bmatrix} v_{Ccd} \\ v_{Ccq} \\ v_{Cc0} \end{bmatrix} \right) \tag{3}$$

$$\omega C_c \begin{bmatrix} -v_{Ccq} \\ v_{Ccd} \\ 0 \end{bmatrix} + C_c \frac{d}{dt} \begin{bmatrix} v_{Ccd} \\ v_{Ccq} \\ v_{Cc0} \end{bmatrix} = - \begin{bmatrix} i_{cd} \\ i_{cq} \\ i_{c0} \end{bmatrix} \tag{4}$$

where ω is the angular frequency of the $d-q-0$ rotating coordinate frame, and is synchronised with the line frequency. When LC-HAPF does not contain L_n ($L_n = 0$), (4) remains the same and (3) becomes

$$\omega L_c \begin{bmatrix} -i_{cq} \\ i_{cd} \\ 0 \end{bmatrix} + L_c \frac{d}{dt} \begin{bmatrix} i_{cd} \\ i_{cq} \\ i_{c0} \end{bmatrix} = \begin{bmatrix} v_{invd} \\ v_{invq} \\ v_{inv0} \end{bmatrix} - \left(\begin{bmatrix} v_d \\ v_q \\ v_0 \end{bmatrix} - \begin{bmatrix} v_{Ccd} \\ v_{Ccq} \\ v_{Cc0} \end{bmatrix} \right) \tag{5}$$

According to (3)–(5), the equivalent circuit models of the three-phase four-wire centre-split LC-HAPF without and with L_n in $d-q-0$ coordinate can be shown in Figs. 1c–f.

2.2 Coupling part filtering characteristics analysis of the LC-HAPF without or with neutral inductor

From Figs. 1c, d and f, L_n will not influence the d, q-coordinate circuit models of the LC-HAPF, but it will influence the 0-coordinate circuit model only. Compared with the 0-coordinate circuit model without L_n as in Fig. 1e,
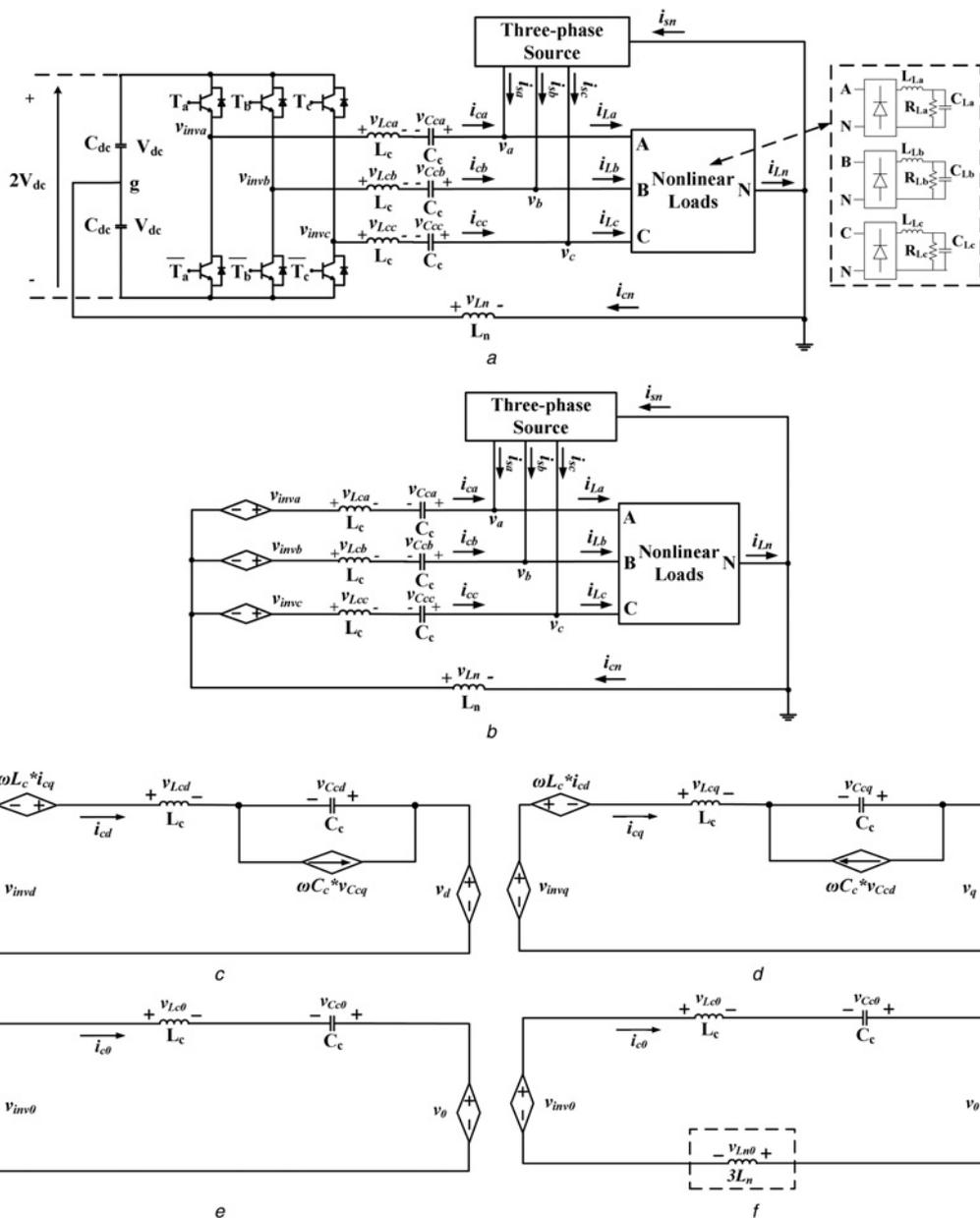
Fig. 1 *Transformerless two-level three-phase four-wire centre-split LC-HAPF*

a Circuit configuration with L_n
b Equivalent circuit model with L_n in $a-b-c$ coordinate
c d-coordinate equivalent circuit model without or with L_n in $d-q-0$ coordinate
d q-coordinate equivalent circuit model without or with L_n in $d-q-0$ coordinate
e 0-coordinate equivalent circuit model without L_n in $d-q-0$ coordinate
f 0-coordinate equivalent circuit model with L_n in $d-q-0$ coordinate

when L_n is added, there is actually an added inductor of $3L_n$ to the 0-coordinate circuit model, as shown in Fig. 1*f*.

From Figs. 1*c*−*e*, without L_n, the resonant frequency of the coupling part of the LC-HAPF in d, q and 0-coordinate circuit models are the same

$$f_{dq\_NL} = f_{0\_NL} = \frac{1}{2\pi\sqrt{L_c C_c}} \quad (6)$$

where f_{dq_NL} and f_{0_NL} are the coupling part resonant frequencies for the LC-HAPF d, q-coordinate circuit models and 0-coordinate circuit model without L_n situation, the subscript '$\_NL$' denotes the system without L_n. This result implies that the coupling part can only possess one resonant

frequency for filtering current harmonics, which can be verified by Fig. 2*a*.

From Figs. 1*c*, *d* and *f*, with L_n, the resonant frequency of the coupling part of the LC-HAPF in d, q and 0-coordinate circuit models can be expressed as

$$f_{dq\_L} = \frac{1}{2\pi\sqrt{L_c C_c}} \quad (7)$$

$$f_{0\_L} = \frac{1}{2\pi\sqrt{(3L_n + L_c)C_c}} \quad (8)$$

where f_{dq_L} and f_{0_L} ($f_{0\_L} < f_{dq\_L}$) are the coupling part resonant frequencies for the LC-HAPF d, q-coordinate
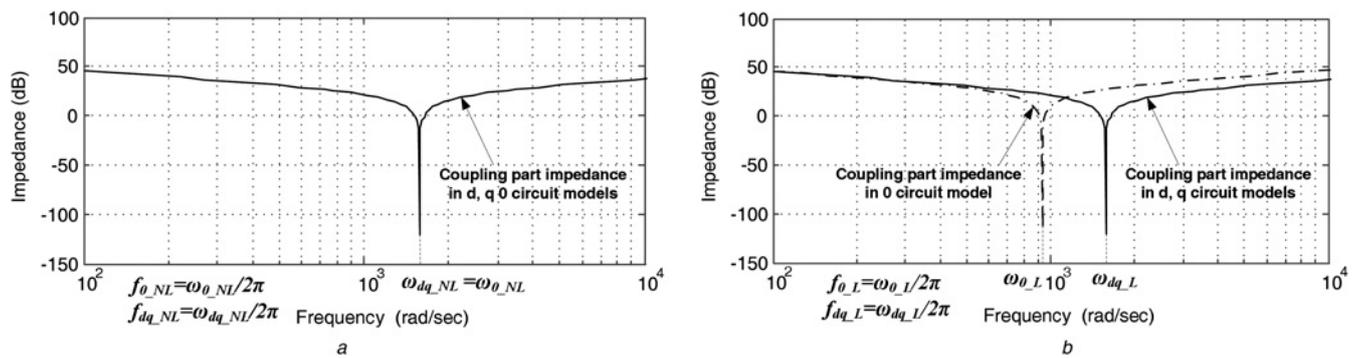
Fig. 2 *Coupling part impedance of the LC-HAPF in $d-q-0$ coordinate circuit models*

a Without L_n
b With L_n

Table 1 Characteristics of the LC-HAPF without and with L_n

LC-HAPF	No. of resonant frequency order for filtering harmonics	No. of LC components		Capacity of the inverter
		L	C	
without L_n	1	3	3	Larger
with L_n	2	4	3	Smaller

Table 2 LC-HAPF system parameters for simulations and experiments

System parameters		Physical values
system source-side	V_x	220 V_{rms}
	F	50 Hz
LC-HAPF	L_c	8 mH
	C_c	50 uF
	C_{dc}	3.3 mF
	V_{dc}	22.5 V, 32.5 V, 45.0 V
	L_n	5 mH
non-linear rectifier load	R_{Lx}	43.2 Ω
	L_{Lx}	34.5 mH
	C_{Lx}	392.0 uF

circuit models and 0-coordinate circuit model with L_n situation, the subscript '_L' denotes the system with L_n. From (7) and (8), it is clearly illustrated that the LC-HAPF can have two different resonant frequencies for filtering current harmonics after the addition of L_n, which can be verified by Fig. 2b. Fig. 2 is plotted based on the LC-HAPF system parameters as in Table 2.

The above analysis clearly shows that the three-phase four-wire centre-split LC-HAPF without and with L_n will have the same d, q-coordinate but different 0-coordinate circuit models. Moreover, the LC-HAPF with L_n can have two different resonant frequencies for harmonic current filtering as indicated by (7) and (8), whereas the LC-HAPF without L_n can only have one as indicated by (6), in which the deduced results based on the circuit models in $d-q-0$ coordinate are equivalent as those deduced through the generic filter structure under positive, negative and zero-sequence analysis [25]. In the following, the resonant frequency selection for the coupling LC without or with L_n will be discussed.

2.3 Resonant frequency selection for coupling LC without or with neutral inductor

Under balanced non-linear loadings consideration, the filtering characteristics and resonant frequency selection for the coupling LC without or with L_n can be determined as follows.

1. When the loading contains $3k$th ($k = 1, 2, \ldots, \infty$) order harmonic current only: Since $3k$th order harmonic current presents in the 0-coordinate circuit model only, the coupling LC without and with L_n can both be tuned at the dominant $3k$th order harmonic frequency (f_{0_NL} and f_{0_L}). From (6) and (8), for $f_{0\_NL} = f_{0\_L}$ consideration, a small L_n can already significantly reduce the size of the three coupling L_c, which benefits for lowering the system initial cost. The coupling LC without and with L_n can only provide one $3k$th order resonant frequency for harmonic current filtering, as indicated by Figs. 1c–f.
2. When the loading contains $3k \pm 1$th order harmonic current only: Since $3k \pm 1$th order harmonic current presents in the d, q-coordinate circuit models only, from Figs. 1c and d, L_n cannot help to improve the coupling part filtering performances under this loading situation. The coupling LC can be tuned at the dominant $3k \pm 1$th order harmonic frequency (f_{dq_NL} and f_{dq_L}). The coupling LC without and with L_n can only provide one $3k \pm 1$th order resonant frequency for harmonic current filtering, as indicated by Figs. 1c–f.
3. When the loading contains any order harmonic current: Since $3k$th and $3k \pm 1$th order harmonic currents can only present in the 0-coordinate and d, q-coordinate circuit models, respectively, the coupling LC with L_n can provide two resonant frequencies for eliminating one $3k$th and one $3k \pm 1$th order harmonic currents, as indicated by Figs. 1c–f. Therefore the coupling LC with L_n can be tuned at one dominant $3k$th and one dominant $3k \pm 1$th order harmonic frequency (f_{dq_L} and f_{0_L}), where the $3k$th order must be smaller than $3k \pm 1$th order.

Owing to wide usage of personal computers, uninterruptible power supplies, high-frequency fluorescent lights, air-conditioning system, various office and consumer electronics equipments in residential, commercial and office buildings, both $3k$th and $3k \pm 1$th order harmonic currents are usually present in those three-phase four-wire distribution power systems [4], thus it is recommended to add a L_n to the LC-HAPF.
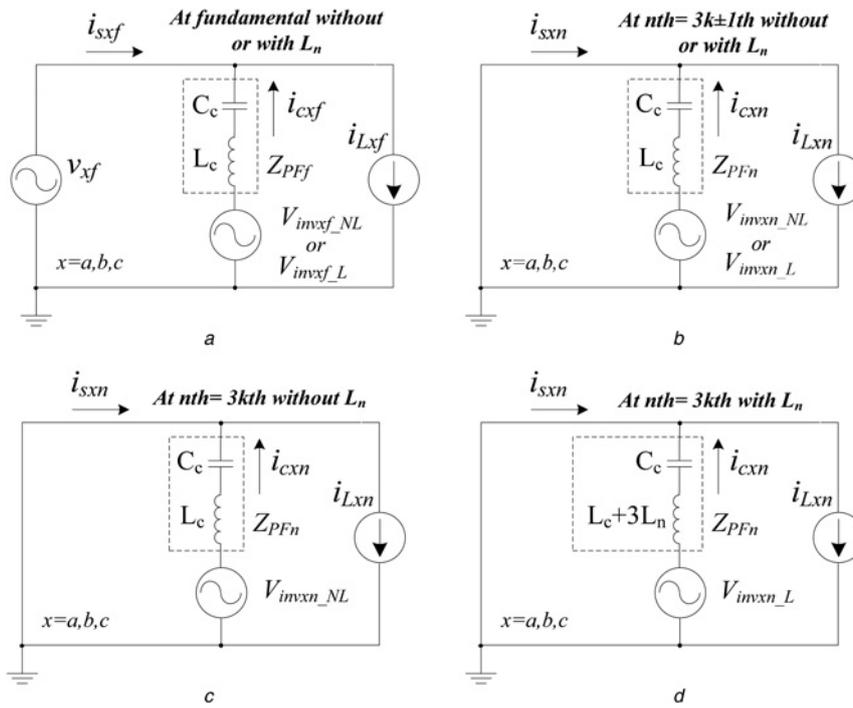
Fig. 3 *LC-HAPF single-phase equivalent circuit model in a−b−c coordinate*

a At fundamental frequency without or with L_n
b At nth $= 3k \pm 1$th harmonic order frequency without or with L_n
c At nth $= 3k$th harmonic order frequency without L_n
d At nth $= 3k$th harmonic order frequency with L_n

Under unbalanced non-linear loadings consideration, both $3k$th and $3k \pm 1$th order harmonic currents can present in the d, q, 0-coordinate circuit models, the coupling LC with L_n can be tuned at two dominant harmonic frequencies (f_{dq_L}, f_{0_L}) and $(f_{0\_L} < f_{dq\_L})$. In the following, the minimum dc-link voltage expressions for the LC-HAPF without and with L_n will be proposed and presented.

3 Minimum inverter capacity analysis of a three-phase four-wire centre-split LC-HAPF

From the previous analysis results, Fig. 3 shows the LC-HAPF single-phase equivalent circuit model in $a−b−c$ coordinate without and with L_n. In the following analysis, all parameters are in root mean square (rms) value. In Fig. 3, the required inverter fundamental output voltages $(V_{invxf\_NL}, V_{invxf\_L})$ and inverter harmonic output voltages $(V_{invxn\_NL}, V_{invxn\_L})$ at each harmonic order can be found, where the subscripts 'f' and 'n' denote the fundamental and harmonic frequency components. As V_{invxf_NL}, V_{invxn_NL}, V_{invxf_L} and V_{invxn_L} are in rms values, the minimum dc-link voltage values $(V_{dcxf\_NL}, V_{dcxn\_NL}, V_{dcxf\_L}, V_{dcxn\_L})$ for compensating the phase fundamental reactive current component and each harmonic current component are calculated as the peak values of the required inverter fundamental and harmonic output voltages, in which $V_{dcxf\_NL} = \sqrt{2}V_{invxf\_NL}$, $V_{dcxn\_NL} = \sqrt{2}V_{invxn\_NL}$, $V_{dcxf\_L} = \sqrt{2}V_{invxf\_L}$ and $V_{dcxn\_L} = \sqrt{2}V_{invxn\_L}$, respectively.

In order to provide sufficient dc-link voltage for compensating load reactive and harmonic currents, the minimum dc-link voltage requirement (V_{dcx_NL}, V_{dcx_L}) of the LC-HAPF single-phase circuit model without and with L_n as shown in (9) and (10) are deduced by considering the worst phase relation between each harmonic component, in

which their corresponding peak voltages of the VSI at AC side are assumed to be superimposed.

$$V_{dcx\_NL} = \sqrt{|V_{dcxf\_NL}|^2 + \sum_{n=2}^{\infty}|V_{dcxn\_NL}|^2} \qquad (9)$$

$$V_{dcx\_L} = \sqrt{|V_{dcxf\_L}|^2 + \sum_{n=2}^{\infty}|V_{dcxn\_L}|^2} \qquad (10)$$

From Fig. 3, as the L_n affects only the $3k$th order harmonic impedance of the coupling part, the LC-HAPF without and with L_n obtain the same fundamental impedance of the coupling part as shown in Fig. 3a. From Fig. 3a, when the load voltage V_x is pure sinusoidal without harmonic components, $V_x = V_{xf}$, the inverter fundamental output voltage of the LC-HAPF single-phase equivalent circuit model without and with L_n can be expressed as

$$V_{invxf\_NL} = V_{invxf\_L} = V_x + Z_{PFf} \times I_{cxf} \qquad (11)$$

As most of the loadings in the distribution power systems are inductive, the fundamental impedance of the coupling capacitor C_c should be larger than that of the coupling inductor L_c, that yields $Z_{PFf} = |Z_{PFf}|e^{j\phi f}$, $(\phi f = -90°)$. When the LC-HAPF operates at ideal case, the fundamental compensating current I_{cxf} contains the pure reactive component I_{cxfq} only without the active current component I_{cxfp}, therefore (11) can be rewritten as

$$V_{invxf\_NL} = V_{invxf\_L} = V_x - \left|\omega L_c - \frac{1}{\omega C_c}\right||I_{cxfq}|, \quad \omega = 2\pi f$$

$$(12)$$

Table 3 Simulated and experimental fundamental reactive current, third, fifth, seventh and ninth orders load harmonic current values

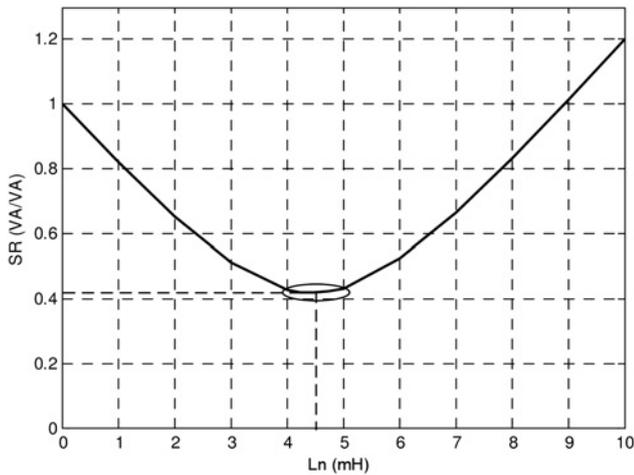|	Fundamental reactive current, A	Third-order harmonic current, A	Fifth-order harmonic current, A	Seventh-order harmonic current, A	Ninth-order harmonic current, A
simulation results	3.72	1.96	0.53	0.23	0.16
experimental results	3.41	1.92	0.45	0.20	0.12

Fig. 4 *Inverter capacity ratio S_R between the LC-HAPF without or with different L_n values*

When the LC-HAPF does not contain L_n, from Figs. 3b and c, the inverter harmonic output voltage V_{invxn_NL} at nth $= 3k \pm 1$th or $3k$th ($k = 1, 2, \ldots, \infty$) harmonic order can be expressed as

$$V_{invxn\_NL} = \left| n\omega L_c - \frac{1}{n\omega C_c} \right| |I_{cxn}|, \qquad n = 2, 3 \ldots \infty \quad (13)$$

where I_{cxn} is the nth order harmonic compensating current.

When the LC-HAPF contains L_n, from Figs. 3b and d, the inverter harmonic output voltage V_{invxn_L} at nth $= 3k \pm 1$th or $3k$th harmonic order can be expressed as (see (14))

When the LC-HAPF is performing compensation, the absolute reactive and nth order harmonic compensating current should be equal to those of the loading, this yields

$$|I_{cxfq}| = |I_{Lxfq}|, \qquad |I_{cxn}| = |I_{Lxn}| \quad (15)$$

where I_{Lxfq} and I_{Lxn} are the reactive and nth order harmonic current of the loading.

From (11)–(15), the inverter fundamental and each nth harmonic order output voltages of the LC-HAPF single-phase circuit model without and with L_n (V_{invxf_NL}, V_{invxn_NL}, V_{invxf_L}, V_{invxn_L}) can be calculated. Then the minimum dc-link voltage requirement (V_{dcx_NL}, V_{dcx_L}) for

the LC-HAPF single-phase circuit model can be found by (9) and (10).

As the LC-HAPF aims to compensate reactive power and current harmonics only but not to provide active power to balance the system current during unbalanced loading case, the generalised single-phase $p-q$ theory is chosen [29] in this paper. By using the single-phase $p-q$ theory, the reactive power and current harmonics in each phase can be compensated independently, thus the final required minimum dc-link voltage for the three-phase four-wire centre-split LC-HAPF without and with L_n (V_{dc_NL}, V_{dc_L}) will be the maximum one among the calculated minimum value of each phase (V_{dcx_NL}, V_{dcx_L}), which are expressed in (16) and (17). Thus, the deduced minimum dc-link voltage expressions can work for both balanced and unbalanced loadings.

$$V_{dc\_NL} = V_{dc} = \max(V_{dca\_NL}, V_{dcb\_NL}, V_{dcc\_NL}) \quad (16)$$

$$V_{dc\_L} = V_{dc} = \max(V_{dca\_L}, V_{dcb\_L}, V_{dcc\_L}) \quad (17)$$

From (16) and (17), the inverter capacity of the LC-HAPF without and with L_n (S_{inv_NL}, S_{inv_L}) can be expressed as

$$S_{inv\_NL} = 3 \frac{V_{dc\_NL}}{\sqrt{2}} I_c \quad (18)$$

$$S_{inv\_L} = 3 \frac{V_{dc\_L}}{\sqrt{2}} I_c \quad (19)$$

where $I_c = \max(I_{ca} = I_{cb} = I_{cc})$. From (18) and (19), the inverter capacity of the LC-HAPF without and with L_n is proportional to their corresponding dc-link voltage. Thus, the dc-link voltage level can reflect the inverter capacity of the LC-HAPF.

Table 6 summarises the minimum dc-link voltage deduction steps of the LC-HAPF without and with L_n. From Table 6, the minimum dc-link voltage value of the LC-HAPF can be calculated only when the spectra of the load currents are known. If the load current spectra cannot be measured (unknown loads) before the installation of the LC-HAPF system, via fast Fourier transform (FFT), the load current spectra can also be figured out by the digital signal processor (DSP) of the LC-HAPF system after installation. Then the minimum dc-link voltage value can be calculated by the DSP through the deduction steps in Table 6. Once the minimum dc-link voltage value is known, the LC-HAPF system can start operation. Through the dc-link voltage control method, the dc-link voltage of

$$V_{invxn\_L} = \begin{cases} V_{invx3k\pm1\_L} = \left| (3k \pm 1)\omega L_c - \dfrac{1}{(3k \pm 1)\omega C_c} \right| |I_{cx3k\pm1}| \\ V_{invx3k\_L} = \left| 3k\omega(L_c + 3L_n) - \dfrac{1}{3k\omega C_c} \right| |I_{cx3k}| \end{cases}, \qquad \begin{array}{l} k = 1, 2 \ldots \infty \\ n = 2, 3 \ldots \infty \end{array} \quad (14)$$

Instantaneous Power Compensation Control Block

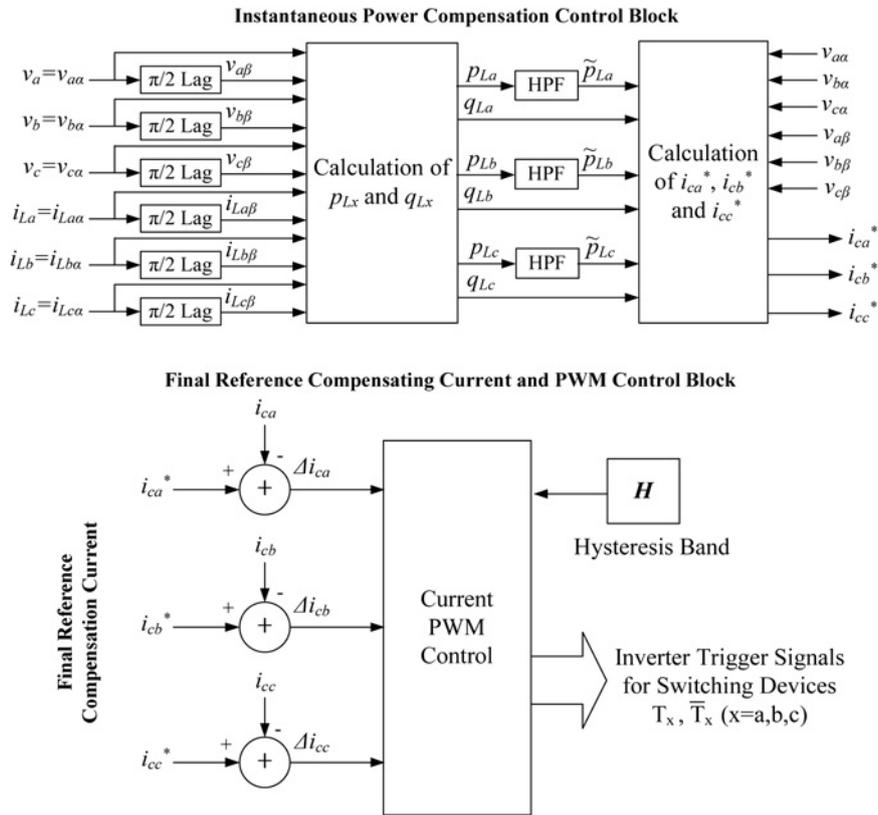**Final Reference Compensating Current and PWM Control Block**

Fig. 5 *Control block diagram for the three-phase four-wire centre-split LC-HAPF*

the LC-HAPF can be controlled to reach this minimum reference value.

For the three single-phase full bridge rectifier loadings as shown in Fig. 1*a* are approximately balanced, from (18) and (19), the inverter capacity ratio S_R between the LC-HAPF with and without L_n can be expressed as

$$S_R = \frac{S_{\text{inv}\_L}}{S_{\text{inv}\_NL}} = \frac{V_{\text{dc}\_L}}{V_{\text{dc}\_NL}} = \frac{V_{\text{dcx}\_L}}{V_{\text{dcx}\_NL}} \qquad (20)$$

As the load harmonic currents are mainly contributed by the third-, fifth-, seventh- and ninth-harmonic orders, the coupling part with L_n are tuned at the fifth- and third-harmonic orders, respectively. For the simulated LC-HAPF system parameters and balanced loading situations as shown in Tables 2 and 3, Fig. 4 shows the S_R between the LC-HAPF without and with different L_n values. From Fig. 4, when L_n is chosen at around 4.5 mH, the minimum inverter capacity of the LC-HAPF can be achieved. Moreover, the inverter capacity of the LC-HAPF with L_n ($L_n = 4$ to 5 mH) can be reduced by more than 50% of that without L_n ($L_n = 0$ mH).

From the above analysis, when the 3*k*th and $3k \pm 1$th order harmonic contents dominate the load harmonic current in a three-phase four-wire system, through appropriate design of the coupling part (L_c, C_c) and L_n, the LC-HAPF with L_n can reduce its inverter capacity compared with the LC-HAPF without L_n. The coupling part is required to be tuned at $3k \pm 1$th order harmonic frequency because the coupling part with L_n can only eliminate the 3*k*th order harmonic current. Moreover, the 3*k*th harmonic order should be smaller than the $3k \pm 1$th harmonic order.

Although the use of the L_n will increase one passive component of the LC-HAPF, it may effectively reduce the

minimum dc-link voltage requirement, so as to lower the LC-HAPF system initial cost. Moreover, since the switching loss is directly proportional to the dc-link voltage [30], the LC-HAPF with L_n will obtain less switching loss if a lower dc-link voltage is used, and vice versa. Besides, the system can also obtain less switching noise, so as to improve its compensation performances. Table 1 summarises the characteristics of the LC-HAPF without and with L_n.

4 Simulation and experimental verifications

In order to verify the filtering characteristics and minimum dc-link voltage analysis in Sections 2 and 3, representative simulation and experimental results of the three-phase four-wire centre-split LC-HAPF system without and with L_n as shown in Fig. 1*a* will be given. The non-linear loads are composed of three single-phase full bridge rectifiers, which act as harmonic producing loads. In order to simplify the verification in this paper, the dc-link is supported by external dc voltage source and the simulated and experimental three-phase loadings are approximately balanced. Table 2 lists the simulated and experimental system parameters for the LC-HAPF. From Table 2, the coupling L_c and C_c are designed based on the load fundamental reactive power consumption and tuned at the fifth-order harmonic frequency, and the coupling part with L_n are tuned at the third-order harmonic frequency. As the simulated and experimental loadings are approximately balanced, only phase *a* compensation diagrams will be illustrated. Simulation studies were carried out by using Matlab.

In order to verify the simulation results, a transformerless two-level three-phase four-wire centre-split LC-HAPF prototype is also implemented in the laboratory. insulated gate bipolar transistors (IGBTs) are employed as the
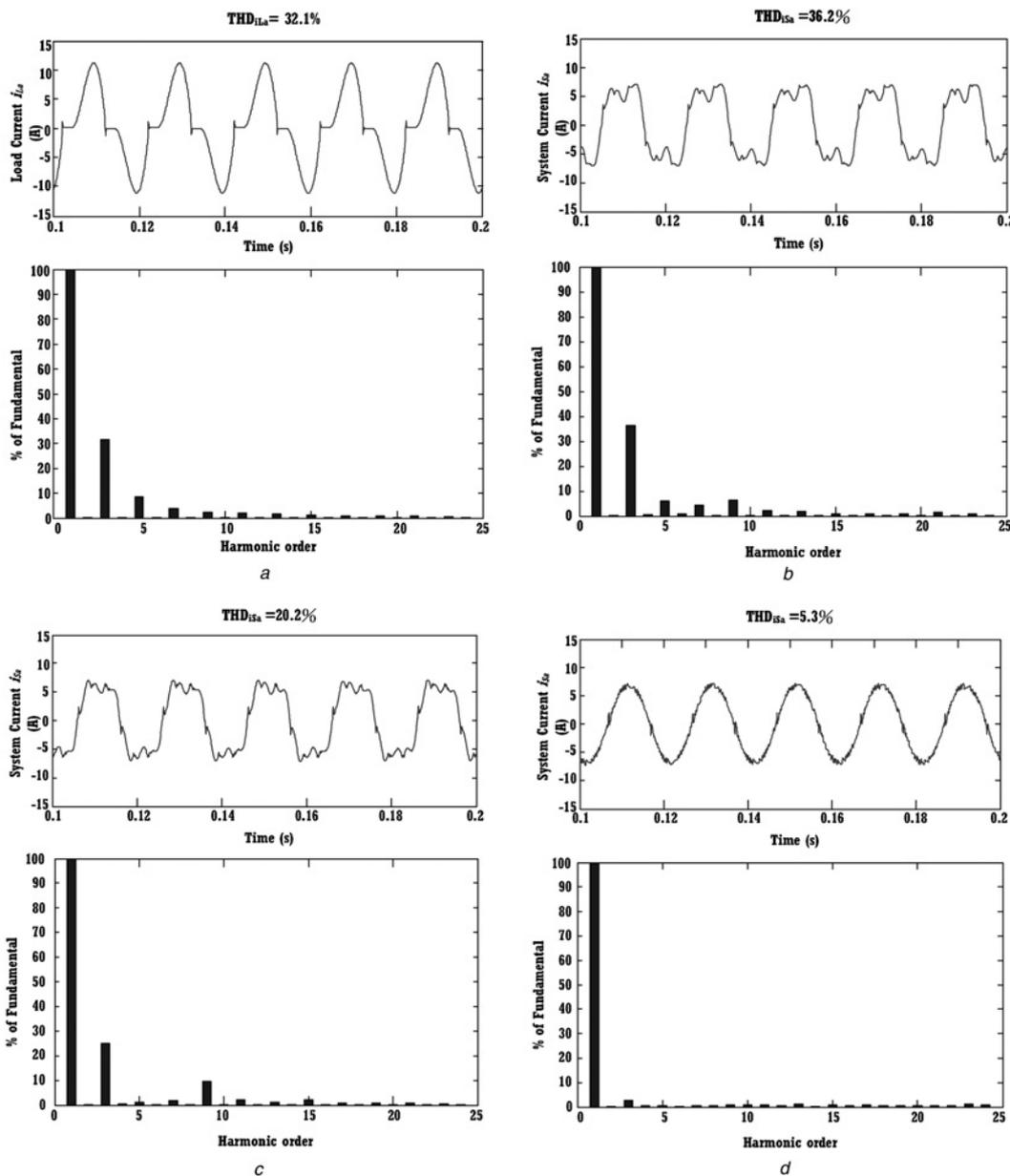
Fig. 6 *Simulated and experimental system current i*$_{sx}$ *and compensating current i*$_{cx}$ *waveforms and their spectra of phase a before and after LC-HAPF compensation*

Simulated results:

a i_{sa} before compensation
b i_{sa} after compensation with $V_{dc} = 22.5$ V ($L_n = 0$)
c i_{sa} after compensation with $V_{dc} = 32.5$ V ($L_n = 0$)
d i_{sa} after compensation with $V_{dc} = 45.0$ V ($L_n = 0$)

switching devices for the active inverter part. And the control system of the prototype is a DSP TMS320F2812 and the analog-to-digital (A/D) sampling frequency of the LC-HAPF system is set at 25 kHz. The three-phase load voltages v_x, load currents i_{Lx} and compensating currents i_{cx} are measured by Hall effect transducers with signal conditioning boards. Then the signal conditioning boards will transfer the large electrical signals (v_x, i_{Lx}, i_{cx}) into small analog signals in order to be adopted as the A/D converter inputs of the DSP. Those signals are necessary to determine the reference compensating currents i_{cx}^* and generate the corresponding i_{cx}. Fig. 5 shows the reactive and harmonic reference compensating current deduction and pulse width modulation (PWM) control block diagram for the three-phase four-wire centre-split LC-HAPF. The instantaneous reference

compensating current i_{cx}^* can be determined by the single-phase p−q theory [29]. Initially, the phase instantaneous active power p_{Lx} and reactive power q_{Lx} are calculated by $p_{Lx} = v_{x\alpha}i_{Lx\alpha} + v_{x\beta}i_{Lx\beta}$ and $q_{Lx} = v_{x\alpha}i_{Lx\beta} - v_{x\beta}i_{Lx\alpha}$. To compensate the reactive power and current harmonics generated by the load, i_{cx}^* for each phase can be calculated by $i_{cx}^* = (1/A_x)[-v_{x\alpha} \cdot \tilde{p}_{Lx} + v_{x\beta} \cdot q_{Lx}]$, where $A_x = v_{x\alpha}^2 + v_{x\beta}^2$. The term $\tilde{p}_{Lx}$ can easily be extracted from p_{Lx} by using a low-pass filter (LPF) or high-pass filter (HPF). After the process of the instantaneous i_{cx}^* determination, the compensating current error Δi_{cx} together with hysteresis band H will be sent to the current PWM control part and the PWM trigger signals for the switching devices of the VSI can then be generated. And this control block diagram will be applied for the LC-HAPF system in
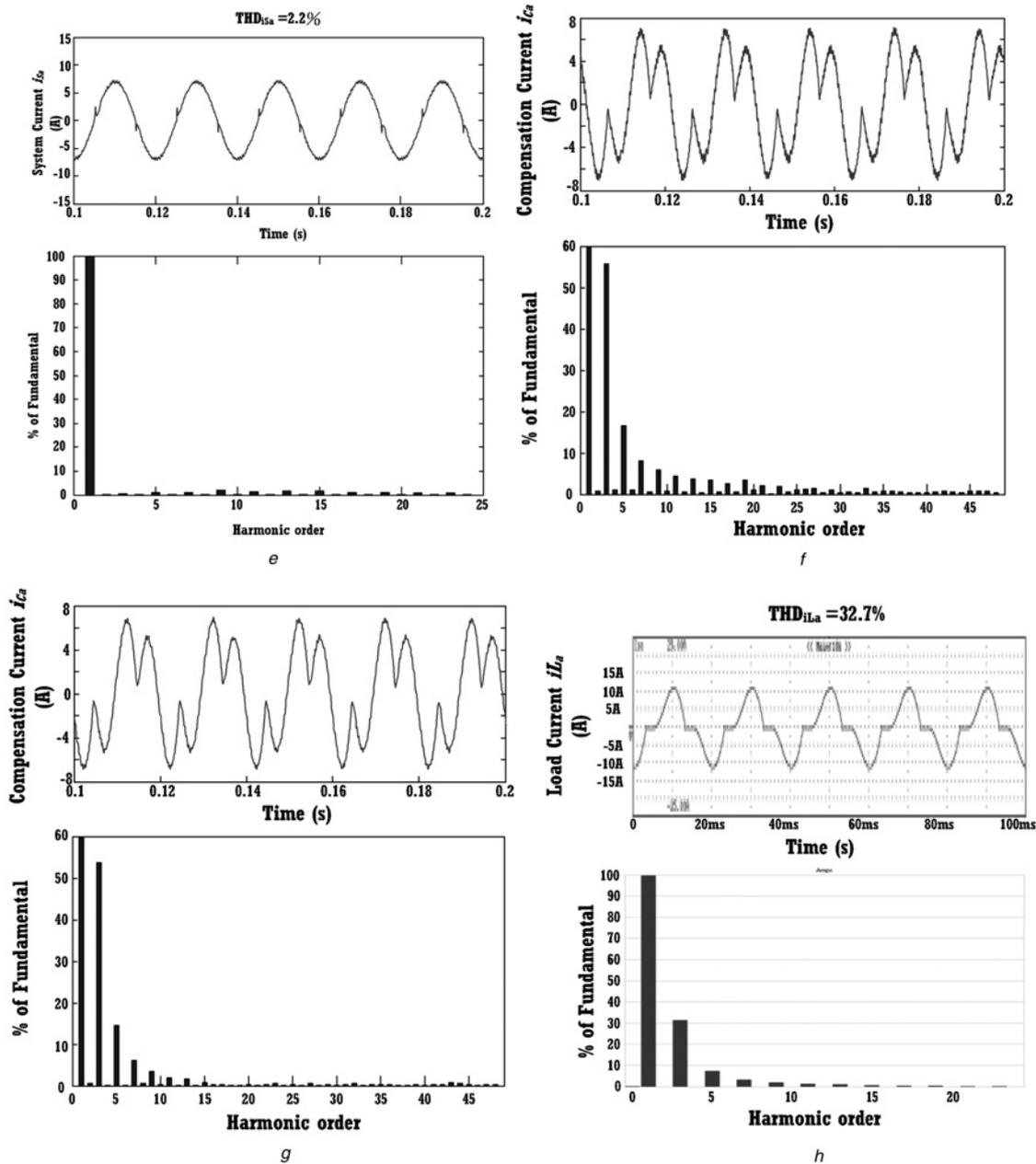
e

f

g

h

Fig. 6 *Continued*

e i_{sa} after compensation with $V_{dc} = 22.5$ V ($L_n = 5$ mH)
f i_{ca} with $V_{dc} = 45.0$ V ($L_n = 0$)
g i_{ca} with $V_{dc} = 22.5$ V ($L_n = 5$ mH)
Experimental results:
h i_{sa} before compensation

order to generate the required compensating current i_{cx}. In the following, since the load harmonic current contents beyond the ninth order are small, for simplicity, the required minimum dc-link voltage calculation will be taken into account up to ninth harmonic order only.

4.1 Simulation results

Fig. 6a illustrates the simulated load current i_{Lx} waveform and its spectrum of phase a, in which its corresponding fundamental reactive current, third-, fifth-, seventh- and ninth-order harmonic current in rms values are shown in Table 3. From Fig. 6a and Table 5, the total harmonic distortion (THD) of the load current ($\text{THD}_{i_{Lx}}$) is 32.1% and the load neutral current (i_{Ln}) is 5.35 A_{rms}, in which the third

(3kth) and fifth (3$k \pm$ 1th) order harmonic contents dominate the load harmonic current. With the help of Table 6, Table 4 shows the required minimum dc-link voltage values (V_{dcxf_NL}, V_{dcxn_NL}, V_{dcxf_L}, V_{dcxn_L}) for compensating the fundamental reactive current, third, fifth, seventh and ninth harmonic current components and the minimum dc-link voltages (V_{dc_NL}, V_{dc_L}) of the LC-HAPF without and with L_n, in which $V_{dc\_NL} = 39.62$ and $V_{dc\_L} = 17.11$ V, respectively. The dc-link voltage for the LC-HAPF is chosen as $V_{dc} = 22.5$, 32.5, 45.0 V three levels for performing compensation, respectively. After compensation by the LC-HAPF without and with L_n, Figs. 6b−e show the simulated system current i_{sx} waveforms and their spectra of phase a at different dc-link voltage levels. Moreover, their corresponding simulation results are summarised in Table 5.
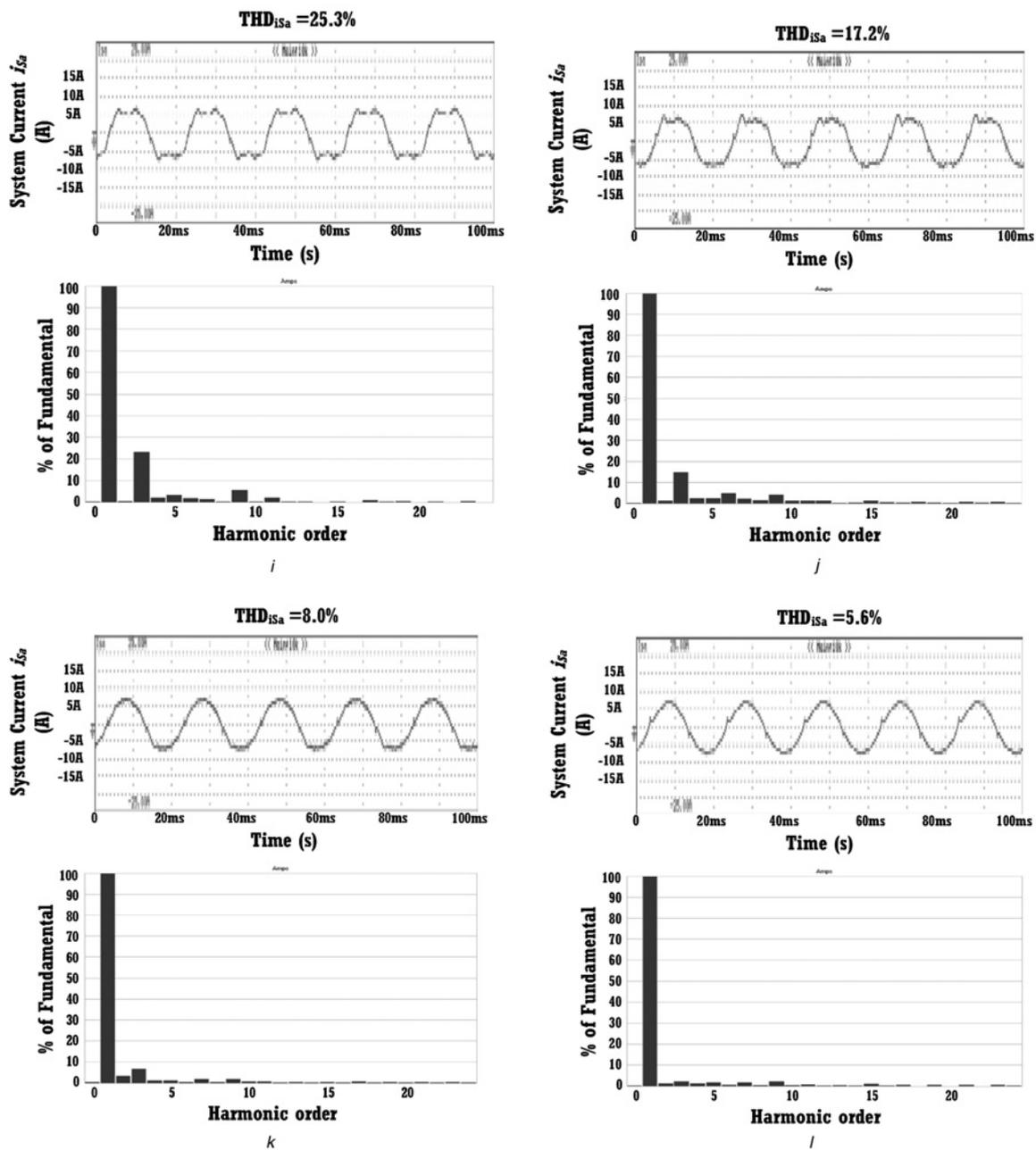
Fig. 6 *Continued*

i i_{sa} after compensation with $V_{dc} = 22.5$ V ($L_n = 0$)
j i_{sa} after compensation with $V_{dc} = 32.5$ V ($L_n = 0$)
k i_{sa} after compensation with $V_{dc} = 45.0$ V ($L_n = 0$)
l i_{sa} after compensation with $V_{dc} = 22.5$ V ($L_n = 5$ mH)

From Table 4, when the LC-HAPF is operating without L_n, the coupling part of the LC-HAPF mainly eliminates the fifth-order harmonic current. From Figs. 6b−e and Table 5, with the dc-link voltage of $V_{dc} = 22.5$ V ($<V_{dc\_NL} = 39.62$ V), the LC-HAPF cannot perform current compensation effectively. After compensation, the THD of phase a system current is THD$_{i_{sx}} = 36.2\%$ and the system neutral current (i_{sn}) is 5.85 A$_{rms}$, in which the compensated THD$_{i_{sx}}$ does not satisfy the international standards (THD$_{i_{sx}} < 16\%$ for IEC, THD$_{i_{sx}} < 20\%$ for IEEE) [31, 32]. When the dc-link voltage increases to $V_{dc} = 32.5$ V, since this value is closer to the required $V_{dc\_NL} = 39.62$ V, the LC-HAPF can obtain better compensating performances with THD$_{i_{sx}} = 20.2\%$ and $i_{sn} = 3.60$ A$_{rms}$, in which the compensated THD$_{i_{sx}}$ still

does not satisfy the international standards [31, 32]. When the dc-link voltage increases to $V_{dc} = 45.0$ V, the LC-HAPF can effectively track the reference compensating current and achieve the best compensation performances with THD$_{i_{sx}} = 5.3\%$ and $i_{sn} = 0.86$ A$_{rms}$ among the three cases. From Table 4, when the LC-HAPF is operating with L_n, the coupling part together with L_n already eliminates the two dominant third and fifth orders harmonic current. Therefore the dc-link voltage of $V_{dc} = 22.5$ V ($>V_{dc\_L} = 17.11$ V) is already sufficient for the LC-HAPF to obtain very good compensating performances with THD$_{i_{sx}} = 2.2\%$ and $i_{sn} = 0.34$ A$_{rms}$, as verified by Fig. 6e and Table 5, in which the compensated THD$_{i_{sx}}$ satisfies the international standards [31, 32].
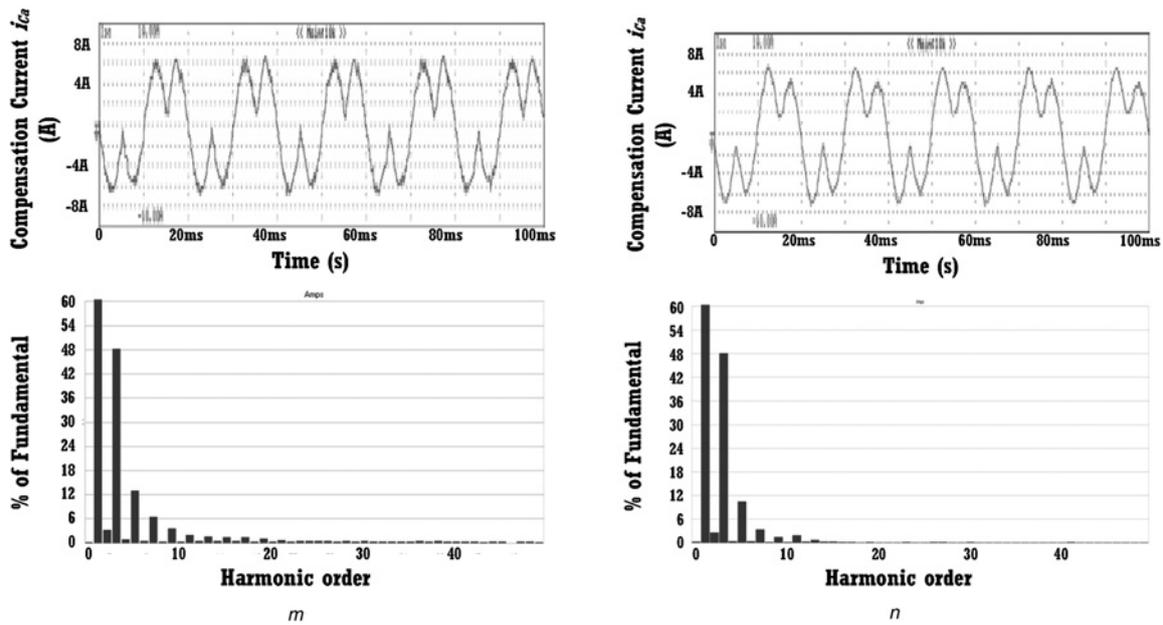
Fig. 6 *Continued*

m i_{ca} with $V_{dc} = 45.0$ V ($L_n = 0$)
n i_{ca} with $V_{dc} = 22.5$ V ($L_n = 5$ mH)

4.2 Experimental results

Fig. 6h illustrates the experimental i_{Lx} waveform and its spectrum of phase *a*, in which its corresponding fundamental reactive current, third, fifth, seventh and ninth load order harmonic current in rms values are shown in Table 3. From Fig. 6h and Table 5, the THD$_{i_{Lx}}$ is 32.7% and the i_{Ln} is 5.77 A$_{rms}$, in which the third (3*k*th) and fifth (3*k* ± 1th) orders harmonic content dominates the load harmonic current. With the help of Table 6, Table 4 shows the required minimum dc-link voltage values (V_{dcxf_NL}, V_{dcxn_NL}, V_{dcxf_L}, V_{dcxn_L}) for compensating the fundamental

reactive current, third, fifth, seventh and ninth harmonic current components and the minimum dc-link voltages of the LC-HAPF without and with L_n, in which $V_{dc\_NL} = 40.77$ V and $V_{dc\_L} = 19.33$ V, respectively. Similar as simulation part, the dc-link voltage for the LC-HAPF is chosen as $V_{dc} = 22.5$, 32.5, 45.0 V three levels for performing compensation, respectively. After compensation by the LC-HAPF without and with L_n, Figs. 6i−l show the experimental i_{sx} waveforms and their spectra of phase *a* at different dc-link voltage levels. Moreover, their corresponding experimental results are summarised in Table 5.

Table 4 Simulated and experimental required dc-link voltage of the LC-HAPF without and with L_n

	LC-HAPF, mH	V_{dcxf_NL}, V_{dcxf_L}, V	V_{dcx3_NL}, V_{dcx3_L}, V	V_{dcx5_NL}, V_{dcx5_L}, V	V_{dcx7_NL}, V_{dcx7_L}, V	V_{dcx9_NL}, V_{dcx9_L}, V	Required V_{dc}, V
simulation results	$L_n = 0$	10.56	37.92	0.13	2.77	3.52	39.62
	$L_n = 5$	10.56	1.26	0.13	2.76	13.11	17.11
experimental results	$L_n = 0$	16.42	37.15	0.10	2.40	2.64	40.77
	$L_n = 5$	16.42	1.24	0.10	2.40	9.83	19.33

Table 5 Summary of simulated and experimental results

LC-HAPF		V_{dc}, V	Third harmonic, %	Fifth harmonic, %	DPF	THD$_{i_{sx}}$, %	i_{sn} (A$_{rms}$)
simulation results	without comp.	–	31.5	8.6	0.80	32.1	5.35
	LC-HAPF ($L_n = 0$ mH)	22.5	36.2	6.1	1.00	36.2	5.85
		32.5	25.2	1.1	1.00	20.2	3.60
		45.0	2.7	0.6	1.00	5.3	0.86
	LC-HAPF ($L_n = 5$ mH)	22.5	0.5	1.0	1.00	2.2	0.34
experimental esults	without comp.	–	31.4	7.3	0.83	32.7	5.77
	LC-HAPF ($L_n = 0$ mH)	22.5	23.8	3.2	1.00	25.3	3.51
		32.5	14.8	2.4	1.00	17.2	2.45
		45.0	6.3	1.1	1.00	8.0	1.30
	LC-HAPF ($L_n = 5$ mH)	22.5	2.4	1.5	1.00	5.6	0.74

From Table 4, when the LC-HAPF is operating without L_n, the coupling part of the LC-HAPF mainly eliminates the fifth order harmonic current. From Figs. 6i–l and Table 5, with $V_{dc} = 22.5$ V ($< V_{dc\_NL} = 40.77$ V), the LC-HAPF cannot perform current compensation effectively. After compensation, the $THD_{i_{sx}}$ of phase a is 25.3% and the i_{sn} is 3.51 A_{rms}, in which the compensated $THD_{i_{sx}}$ does not satisfy the international standards [31, 32]. When the dc-link voltage increases to $V_{dc} = 32.5$ V, since this value is closer to the required $V_{dc\_NL} = 40.77$ V, the LC-HAPF can obtain better compensating performances with $THD_{i_{sx}} = 17.2\%$ and $i_{sn} = 2.45$ A_{rms}, in which the compensated $THD_{i_{sx}}$ still does not satisfy the IEC standard [32]. When the dc-link voltage increases to $V_{dc} = 45.0$ V, the LC-HAPF can achieve the best compensation performances with $THD_{i_{sx}} = 8.0\%$ and $i_{sn} = 1.30$ A_{rms} among the three cases. From Table 4, when the LC-HAPF is operating with L_n, the coupling part together with L_n already eliminates the two dominant third- and fifth-orders harmonic current. Therefore the dc-link voltage of $V_{dc} = 22.5$ V ($> V_{dc\_L} = 19.33$ V) is already sufficient to obtain very good compensating performances with $THD_{i_{sx}} = 5.6\%$ and $i_{sn} = 0.74$ A_{rms}, as verified by Fig. 6l and Table 5, in which the compensated $THD_{i_{sx}}$ satisfies the international standards [31, 32].

The experimental results are similar to the simulated results, which verified the previous analyses of the LC-HAPF filtering characteristics and minimum dc-link voltage requirement. In order to obtain good compensating performances for the LC-HAPF, the dc-link operating voltage can be chosen as the calculated minimum dc-link voltage (V_{dc_NL}, V_{dc_L}). From the simulation and experimental results, the required dc-link voltages for the LC-HAPF with L_n can have a great reduction of more than 50% compared with those without L_n. Since the dc-link operating voltage reflects the inverter capacity, the LC-HAPF with L_n can significantly reduce its inverter capacity. Besides, it can also reduce the switching loss as the switching loss is directly proportional to the dc-link voltage [30], in which the experimental inverter power loss (W) of the LC-HAPF with L_n ($V_{dc} = 22.5$ V) can be reduced by more than 5.0% than that of the LC-HAPF without L_n ($V_{dc} = 45.0$ V).

Figs. 6f and g and Figs. 6m and n show the LC-HAPF simulated and experimental compensating current i_{cx} waveforms and their spectra of phase a with $V_{dc} = 45.0$ V (without L_n) and $V_{dc} = 22.5$ V (with $L_n = 5$ mH). From Figs. 6f and g and Figs. 6m and n, since the i_{ca} harmonic contents above 15th harmonic order (switching noise) shows a significant reduction by adding a L_n, thus the LC-HAPF with L_n can effectively reduce the switching noise and also improve the compensation performances as verified by Table 5, in comparison with the conventional LC-HAPF without L_n, because it just requires a lower dc-link voltage requirement for performing compensation.

Without L_n case, if the coupling L_c and C_c are tuned at third-order harmonic frequency instead of fifth order, the dc-link voltage reduction with L_n may not be so significant. Unfortunately, by tuning L_c and C_c at third order harmonic frequency, it will significantly increase the initial cost and size of the LC-HAPF, because the required three coupling L_c will be increased from 8 to 22.5 mH, compared with the coupling L_c and C_c tuned at fifth order with a L_n of 5 mH only.

If 3kth order load harmonic current exists, by concerning about (i) initial costs of both the passive part (L_c and C_c) and inverter part (dc-link voltage) and (ii) switching loss

and switching noise, it is cost effective for the coupling part of the LC-HAPF with L_n to be tuned at one dominant 3kth and one dominant $3k \pm 1$th order harmonic currents (3kth $< 3k \pm 1$th).

5 Conclusion

This paper aims to investigate the minimum inverter capacity design for three-phase four-wire centre-split LC LC-HAPF. Firstly, the equivalent circuit models of the three-phase four-wire centre-split LC coupling hybrid active power filters (LC-HAPF) in $d-q-0$ coordinate are built and proposed. Based on the circuit models, the triplen harmonic filtering performance of the LC-HAPF can be improved by adding a tuned neutral inductor. After that, the minimum dc-link voltage expressions for the LC-HAPF without and with neutral inductor are also deduced, which can work for both balanced and unbalanced loadings. According to the current quality of the loading and the minimum dc-link voltage expressions, the dc-link voltage reduction analysis for the LC-HAPF with neutral inductor can be mathematically obtained. Thus, the initial cost, switching loss and switching noise of the LC-HAPF can be lowered by the additional neutral inductor. Finally, simulation and experimental results of the three-phase four-wire centre-split LC-HAPF with neutral inductor are presented to verify its filtering characteristics and the deduced minimum dc-link voltage expressions, and to show the effectiveness of reducing its dc-link voltage requirement (inverter capacity), switching loss, switching noise and improving the system performances in current quality compensation compared with the conventional LC-HAPF without neutral inductor.

6 Acknowledgment

7 References

1 Subjek, J.S., Mcquilkin, J.S.: 'Harmonics-causes, effects, measurements and analysis', *IEEE Trans. Ind. Electron.*, 1990, **26**, (6), pp. 1034–1042
2 Duarte, L.H.S., Alves, M.F.: 'The degradation of power capacitors under the influence of harmonics'. Proc. IEEE 10th Int. Conf. on Harmonics and Quality of Power, 2002, vol. 1, pp. 334–339
3 Tran, T.Q., Conrad, L.E., Stallman, B.K.: 'Electric shock and elevated EMF levels due to triplen harmonics', *IEEE Trans. Power Del.*, 1996, **11**, (2), pp. 1041–1049
4 Quinn, C.A., Mohan, N.: 'Active filtering of harmonic currents in three-phase, four-wire systems with three-phase and single-phase nonlinear loads'. Proc. IEEE Seventh Annual Applied Power Electronics Conf. and Exposition, APEC. 92, 1992, pp. 829–836
5 Singh, B., Al-Haddad, K., Chandra, A.: 'A review of active filters for power quality improvement', *IEEE Trans. Ind. Electron.*, 1999, **46**, (5), pp. 960–971
6 de Camargo, R.F., Picheiro, H.: 'Three-phase four-wire shunt active filter to reduce voltage and current distortions in distribution systems'. Proc. IEEE 32nd Annual Conf. on Industrial Electronics, IECON. 06, 2006, pp. 1884–1889
7 Senini, S.T., Wolfs, P.J.: 'Systematic identification and review of hybrid active filter topologies'. Proc. IEEE 33rd Annual Power Electronics Specialists Conf., PESC. 02, 2002, vol. 1, pp. 394–399
8 Salmerón, P., Litrán, S.P.: 'A control strategy for hybrid power filter to compensate four-wires three-phase systems', *IEEE Trans. Power Electron.*, 2010, **25**, (7), pp. 1923–1931
9 Luo, A., Zhao, W., Deng, X., Shen, Z.J., Peng, J.-C.: 'Dividing frequency control of hybrid active power filter with multi-injection branches using improved i_p-i_q algorithm', *IEEE Trans. Power Electron.*, 2009, **24**, (10), pp. 2396–2405

10 Luo, A., Shuai, Z.K., Shen, Z.J., Zhu, W.J., Xu, X.Y.: 'Design considerations for maintaining dc-side voltage of hybrid active power filter with injection circuit', *IEEE Trans. Power Electron.*, 2009, **24**, (1), pp. 75–84

11 Peng, F.Z., Akagi, H., Nabae, A.: 'A new approach to harmonic compensation in power systems – a combined system of shunt passive and series active filters', *IEEE Trans. Ind. Appl.*, 1990, **26**, (6), pp. 983–990

12 Kawahira, H., Nakamura, T., Nakazawa, S., Nomura, M.: 'Active power filter'. Proc. IPEC-Tokyo, 1983, pp. 981–992

13 Villalva, M.G., Ruppert, E.F.: 'Four-wire shunt active power filter with adaptive selective current compensation'. Proc. IEEE 36th Power Electronics Specialists Conf., PESC. 05, 2005, pp. 347–353

14 Luo, A., Tang, C., Shuai, Z.K., Zhao, W., Rong, F., Zhou, K.: 'A novel three-phase hybrid active power filter with a series resonance circuit tuned at the fundamental frequency', *IEEE Trans. Ind. Electron.*, 2009, **56**, (7), pp. 2431–2440

15 Fujita, H., Akagi, H.: 'A practical approach to harmonic compensation in power systems – series connection of passive and active filters', *IEEE Trans. Ind. Appl.*, 1991, **27**, (6), pp. 1020–1025

16 Park, S., Sung, J.-H., Nam, K.: 'A new parallel hybrid filter configuration minimizing active filter size'. Proc. IEEE 30th Annual Power Electronics Specialists Conf., PESC. 99, 1999, vol. 1, pp. 400–405

17 Rivas, D., Moran, L., Dixon, J.W., Espinoza, J.R.: 'Improving passive filter compensation performance with active techniques', *IEEE Trans. Ind. Electron.*, 2003, **50**, (1), pp. 161–170

18 Fujita, H., Yamasaki, T., Akagi, H.: 'A hybrid active filter for damping of harmonic resonance in industrial power systems', *IEEE Trans. Power Electron.*, 2000, **15**, (2), pp. 215–222

19 Akagi, H.: 'New trends in active filters for power conditioning', *IEEE Trans. Ind. Appl.*, 1996, **32**, (6), pp. 1312–1322

20 Tangtheerajaroonwong, W., Hatada, T., Wada, K., Akagi, H.: 'Design and performance of a transformerless shunt hybrid filter integrated into a three-phase diode rectifier', *IEEE Trans. Power Electron.*, 2007, **22**, (5), pp. 1882–1889

21 Inzunza, R., Akagi, H.: 'A 6.6-kV transformerless shunt hybrid active filter for installation on a power distribution system', *IEEE Trans. Power Electron.*, 2005, **20**, (4), pp. 893–900

22 Srianthumrong, S., Akagi, H.: 'A medium-voltage transformerless ac/dc Power conversion system consisting of a diode rectifier and a shunt hybrid filter', *IEEE Trans. Ind. Appl.*, 2003, **39**, (3), pp. 874–882

23 Lam, C.-S., Choi, W.-H., Wong, M.-C., Han, Y.-D.: 'Adaptive dc-link voltage controlled hybrid active power filters for reactive power compensation', *IEEE Trans. Power Electron.*, 2012, **27**, (4), pp. 1758–1772

24 Jou, H.-L., Wu, K.-D., Wu, J.-C., Li, C.-H., Huang, M.-S.: 'Novel power converter topology for three phase four-wire hybrid power filter', *IET Power Electron.*, 2008, **1**, (1), pp. 164–173

25 Rodriguez, P., Candela, J.I., Luna, A., Asiminoaei, L., Teodorescu, R., Blaabjerg, F.: 'Current harmonics cancellation in three-phase four-wire systems by using a four-branch star filtering topology', *IEEE Trans. Power Electron.*, 2009, **24**, (8), pp. 1939–1950

26 Lam, C.-S., Wong, M.-C., Han, Y.-D.: 'Voltage swell and overvoltage compensation with unidirectional power flow controlled dynamic voltage restorer', *IEEE Trans. Power Del.*, 2008, **23**, (4), pp. 2513–2521

27 Hiti, S., Boroyevich, D., Cuadros, C.: 'Small-signal modeling and control of three-phase PWM converters'. Conf. Record of the Industry Applications Society Annual Meeting, 1994, vol. 2, pp. 1143–1150

28 Richard, Z.: 'High performance power converter systems for nonlinear and unbalanced load/source'. Ph.D. thesis, Virginia Polytechnic Institute and State University, 1998

29 Khadkikar, V., Chandra, A., Singh, B.N.: 'Generalized single-phase p-q theory for active power filtering: simulation and DSP-based experimental investigation', *IET Power Electron.*, 2009, **2**, pp. 67–78

30 Wong, M.-C., Tang, J., Han, Y.-D.: 'Cylindrical coordinate control of three-dimensional PWM technique in three-phase four-wired trilevel inverter', *IEEE Trans. Power Electron.*, 2003, **18**, (1), pp. 208–220

31 IEEE Standard 519-1992: 'IEEE Recommended Practices and Requirements for Harmonic Control in Electrical Power Systems', 1992

32 IEC Standard 61000-3-2: 'Electromagnetic Compatibility (EMC), Part 3: Limits, Section 2: Limits for Harmonics Current Emissions (Equipment Input Current ≤16A Per Phase)', 1997

8 Appendix

Table 6 summarises the minimum dc-link voltage deduction steps of the LC-HAPF without and with L_n.

Table 6 Minimum dc-link voltage deduction steps of the LC-HAPF without and with L_n

---

1 inverter fundamental output voltage without and with L_n

$$V_{invxf\_NL} = V_{invxf\_L} = V_x - \left| \omega L_c - \frac{1}{\omega C_c} \right| |I_{cxfq}| \qquad (12)$$

where $|I_{cxfq}| = |I_{Lxfq}|$, $\omega = 2\pi f$

2 inverter nth harmonic order output voltage without and with L_n

$$V_{invxn\_NL} = \left| n\omega L_c - \frac{1}{n\omega C_c} \right| |I_{cxn}| \qquad (13)$$

$$V_{invxn\_L} = \begin{cases} V_{invx3k\pm1\_L} = \left| (3k \pm 1)\omega L_c - \frac{1}{(3k \pm 1)\omega C_c} \right| |I_{cx3k\pm1}| \\ V_{invx3k\_L} = \left| 3k\omega(L_c + 3L_n) - \frac{1}{3k\omega C_c} \right| |I_{cx3k}| \end{cases}$$

$$(14)$$

where $|I_{cxn}| = |I_{Lxn}|$, $nth = 3k \pm 1$th or $3k$th, $k = 1, 2, \ldots, \infty$, $n = 2, 3, \ldots, \infty$, $\omega = 2\pi f$

3 minimum dc-link voltage without L_n

$$V_{dc\_NL} = V_{dc} = \max(V_{dca\_NL}, V_{dcb\_NL}, V_{dcc\_NL}) \qquad (16)$$

where

$$V_{dcx\_NL} = \sqrt{|V_{dcxf\_NL}|^2 + \sum_{n=2}^{\infty} |V_{dcxn\_NL}|^2} \qquad (9)$$

$V_{dcxf\_NL} = \sqrt{2} V_{invxf\_NL}$, $V_{dcxn\_NL} = \sqrt{2} V_{invxn\_NL}$, where $n = 2, 3, \ldots, \infty$

minimum dc-link voltage with L_n

$$V_{dc\_L} = V_{dc} = \max(V_{dca\_L}, V_{dcb\_L}, V_{dcc\_L}) \qquad (17)$$

where

$$V_{dcx\_L} = \sqrt{|V_{dcxf\_L}|^2 + \sum_{n=2}^{\infty} |V_{dcxn\_L}|^2} \qquad (10)$$

$V_{dcxf\_L} = \sqrt{2} V_{invxf\_L}$, $V_{dcxn\_L} = \sqrt{2} V_{invxn\_L}$, where $n = 2, 3, \ldots, \infty$